Heliyon 9 (2023) e13223

Contents lists available at ScienceDirect

Heliyon

journal homepage: www.cell.com/heliyon

Research article

Adsorption efficacy of functionalized Cu-BDC MOFs tethered 2-mercaptobenzimidazole analogue: A comparative study

Malathi Challa [a,*], Sampath Chinnam [a], Ambika Madalakote Rajanna [b], Apurva Nandagudi [c], Basappa C. Yallur [a], Vinayak Adimule [d]

[a] Department of Chemistry, M. S. Ramaiah Institute of Technology (Affiliated to Visvesvaraya Technological University, Belgaum), Bengaluru, Karnataka 560054, India
[b] Department of Physics, M. S. Ramaiah Institute of Technology (Affiliated to Visvesvaraya Technological University, Belgaum), Bengaluru, Karnataka 560054, India
[c] Department of Science & Humanities, PES University, Bengaluru 560085, Karnataka, India
[d] Angadi Institute of Technology and Management (AITM), Savagaon Road, Belagavi 591108, Karnataka, India

ARTICLE INFO

Keywords:
2-Mercaptobenzimidazole analogue
Cu-BDC MOFs
Congo red
Adsorption

ABSTRACT

A novel metal-organic framework [MOFs], and 2-[benzo [*d*]thiazol-2-ylthio)-3-hydroxy acrylaldehyde-Cu-benzene dicarboxylic acid was synthesized by solvothermal method and characterized using *p*-XRD, FSEM-EDX, TGA, BET, FTIR. The tethered organic linker, 2-[benzo [*d*] thiazol-2-ylthio)-3-hydroxyacrylaldehyde was commonly known as 2-mercaptobenimidazole analogue [2-MBIA]. Analysis of BET disclosed that addition of 2-MBIA to Cu-benzene dicarboxylic acid [Cu-BDC], reduced the crystallite size from 70.0 nm to 65.90 nm, surface area from 17.95 to 17.02 $m^2\ g^{-1}$ and enhances the pore size from 5.84 nm with 0.027 $cm^3\ g^{-1}$ pore volume to 8.74 nm with 0.361 $cm^3\ g^{-1}$ pore volume. Batch experiments were conducted to optimize pH, adsorbent dosage, and, Congo red (CR) concentration. The adsorption percentage of CR on the novel MOFs was 54%. Adsorption kinetic studies revealed that the uptake adsorption capacity at equilibrium was 184.7 mg/g from pseudo-first-order kinetics which gave a good fit with the experimental data. Intraparticle diffusion model explained the process of the adsorption mechanism: diffusion from the bulk solution onto the porous surface of the adsorbent. Freundlich and Sips models were the best fit models of the several non-linear isotherm models. Temkin isotherm suggested the adsorption of CR on MOFs was of an exothermic nature.

1. Introduction

Organic dyes find application in several fields like food, leather, textile, and printing fields that generally affect the ecosystem as they contribute to a greater extent to the contamination of water [1,2]. Congo red is a benzidine-based diazo dye that is highly biodegradable at –N═N- and resistant to further degradation to CO_2 and H_2O due to the presence of an aromatic structure by fungus [*Aspergillus flavus* JKSC-7, *Caldariomyces fumago*] *via* enzymatic degradation [3,4]. In general, Congo red is considered a carcinogen and major pollutant so the ecosystem demands the removal of such components from water [5,6]. To achieve this, researchers made efforts into using different methods like reverse osmosis, advanced oxidation, photocatalytic, ozonation, coagulation/flocculation,

* Corresponding author.
E-mail addresses: maalathichalla@msrit.edu, maalathichalla@gmail.com (M. Challa).

https://doi.org/10.1016/j.heliyon.2023.e13223
Received 1 August 2022; Received in revised form 19 January 2023; Accepted 20 January 2023
Available online 24 January 2023

adsorption, precipitation, biodegradation, etc. Among all these methods, adsorption is simple, cost-effective, with high efficiency. Research has been in progress for the removal of pollutants by using several materials like metals, nano metal oxides, activated carbon, carbon nanotubes, silica gel, zeolite, and metal-organic frameworks [7].

The MOFs are attracted by several researchers from the last vicennial period due to their potential properties like surface area, shape, and pore size. Furthermore, researchers can systematically modify the three-dimensional hybrid structures and functional groups of MOFs [8–11], which aids in the achievement of the desired goals. MOFs are the new alternate adsorbents with cost-effective, high thermal stability, change of porosity size, and metal sites [12]. Several organic linkers which consist of heterocyclic compounds like pyridine, pyrazole, imidazole, and triazole rings along with the carboxyl group play a vital role to establish hydrogen bonding; also, a π−π stacking interaction sites between MOFs and the organic pollutant, therefore, enables adsorption process [13]. In the literature survey, a comparative study on the adsorption efficiency of Mn-UiO-66, GONH2, and Mn-UiO-66@GO-NH_2 composites revealed that CR adsorption was 243.08, 292.99, and 486.17 mg/g respectively for 120 min with 50 mL of 100 ppm Congo red and 10 mg of adsorbents [14]. Similarly, the influence of the organic linker moieties on the adsorption efficiency of Cd-MOFs ([Cd (5-aip) (bpy)] (1) and [Cd (5-hip) (bpy)]) was found 98.58% and 98.93% of CR for 24 h. Time consumption was the drawback of these studies [15]. Several researchers aim to study only the adsorption process involved but do not discuss it in detail. For a better understanding of the adsorption mechanism, non-linear kinetics and isotherm models are very much required [16].

In this pursuit, an attempt has been made in the present study to compare the adsorption mechanism and efficacy of novel MOFs with Cu-BDC MOFs in detail by applying different nonlinear kinetic and isotherms models and has given importance to reducing the time consumption. Optimization studies have been conducted for pH, time, adsorbent dosage, and dye concentration effect on the sorption capacity of current MOFs synthesized [17–21].

2. Experimental

2.1. Materials

All the chemicals and reagents were purchased from Sigma Aldrich, SD Fine Chemical Ltd. Avra Synthesis Private, Ltd. India and utilized as such without any purification. Cu $(NO_3)_2{\cdot}3H_2O$ 98%, and sodium oxalate >99.5% (Sigma-Aldrich), Terephthalic acid 98% (Avra Synthesis Private Ltd), N, *N*-dimethyl formamide (DMF) (Spectro chem Ltd>97.5%), sodium hydroxide (NaOH, SD-Fine Chemicals Ltd.>97.5%) 2- Alfa Asear,>99%).

2.2. Synthesis of [2-mbia-Cu-BDC] MOFs

2-MBIA-Cu-BDC MOFs was synthesized using the solvothermal method. 0.01 M of Cu $(NO_3)_2{\cdot}3H_2O$ was dispersed in 50 mL of dimethylformamide (DMF) containing the equimolar (0.01 M) mixture of H_2BDC and 2-MBIA in the beaker and kept stirring at room temperature for 30 min. Further, the mixture was kept under slow heating in a stainless-steel hydrothermal bomb at the rate of 5 °C/min to attain the temperature of the oven around 125 °C and placed for 2 days [22]. Later, the solid MOFs was filtered, washed with DMF, water, and dried at 80–110 °C for 24 h to remove adsorbed solvent molecules. The yield of 2-MBIA-Cu-BDC MOFs was 78.14%. The same procedure was followed to synthesize Cu-BDC MOFs with a yield of 62%.

2.3. Characterization

The stretching and bending vibrations of both MOFs were investigated using Fourier transformed Infrared spectrum (FTIR) (Bruker-Alpha, Germany) and X-ray Diffractometer (Bruker D8 advance diffractometer) was used to characterize both MOFs. The morphology of both MOFs was analyzed using Scanning Electron Microscope. Thermograms were recorded using a Thermogravimetric analyzer (NETZSCH STA 449 F5). BET analysis was performed by BET analyzer (BELSORP MR1). Adsorption studies were carried out using Systronics double beam spectrophotometer 2202.

2.4. Adsorption studies

Adsorption studies was carried out using 10 mg of MOFs added to the aqueous solutions (100 ppm) of the different dyes like Indigo carmine (IGC), Congo Red (CR), and Martins yellow (MY) which were kept stirring for 30 min and measured the concentration of each dye by UV–Vis Systronics double beam spectrophotometer 2202. Of the three, CR was found to be highly adsorbed on newly synthesized 2-MBIA-Cu-BDC MOFs which may be attributed to π-π interaction/electrostatic attraction, and also its pore size. Thus, CR was selected as the standard dye to investigate the adsorption efficacy of both MOFs at 490 nm (λ_{max}).

For optimization of the adsorption conditions concerning sorption kinetic studies and adsorption isotherms, a systematic study was conducted batch-wise: (i) different pH (2–10) solutions (ii) different dosages of adsorbent (10–50 mg) (iii) different dye concentrations (10–150 ppm) and iv) effect of time (10 min–180 min). Further, all these samples were centrifuged and absorbance was measured. The pseudo-first-order, pseudo-second-order, Elovich, and diffusion models were used to analyze the kinetic model and adsorption mechanism. Five adsorption isotherm models viz Langmuir, Freundlich, Temkin, (two parameters) Sips and Redlich -Peterson isotherm (three parameters) in their nonlinear forms were employed for unfolding adsorption efficacy of the current MOFs [23–25].

2.5. Statistical analysis

Non-linear least square analysis was employed to fit the experimental data for the selected modelling of isotherms and kinetics with the support of the SOLVER tool based on the Generalized Reduced Gradient (GRG) method of iteration available in Microsoft Exc. The residual sum of square (RSS), the coefficient determination (R^2), Chi-square (χ^2), and average relative error (ARE) were considered to find the best fit kinetic and isotherm models. All the parameters were calculated from the below equations [26,45,49].

$$R^2 = \frac{\Sigma(q_{e,pre,i} - q_{e,exp,avg})^2}{\Sigma(q_{e,pre,i} - q_{e,exp,avg})^2 - \Sigma(q_{e,pre,i} - q_{e,exp,i})^2} \quad (1)$$

$$RSS = \sum_{i=1}^{N} (q_{e,exp,i} - q_{e,pre,i})^2 \quad (2)$$

$$ARE = \frac{100}{N} \sum_{i=1}^{N} \frac{(q_{e,pre,i} - q_{e,exp,i})}{q_{e,exp,i}} \quad (3)$$

$$\chi^2 = \sum_{i=1}^{N} \frac{(q_{e,exp,} - q_{e,pre})^2}{q_{e,exp}} \quad (4)$$

3. Results and discussion

3.1. XRD diffraction analysis

Cu-BDC MOFs diffractogram peaks were observed at 2θ values of 10.23°(001),12.16° (011), 15.51°(101), 17.24° (121), 20.53° (211), 22.04°(−102), 24.91°(020), 29.10°(232), 31.26°(003) 33.16°, 36.40°, 39.76°, 42.35°, 45.86°, 46.82°, 50.77°, 53.03°, 56.65° and 2-MBIA-Cu-BDC MOFs diffractogram peaks were noticed at 2θ values of 10.27°(001), 12.17°(011), 16.97°(011), 17.25°(121), 17.84°(0–10), 20.53°(211), 22.04°(−102), 24.91°(020), 25.46°(−102), 25.45°(−100) 29.21°(232), 30.92°, 33.29°, 34.18°,36.42°, 39.02°, 42.86°, 44.31°, 47.06°, 51.03°, 51.72°, 56.34°, 60.08°,66.52°, 68.68° as shown in Fig. 1 and were in good agreement with the literature [1,27]. Debye–Scherrer's equation (5) [9,50] was used to calculate the average crystallite size of Cu-BDC MOFs was 70 nm and 65.9 nm for 2-MBIA-Cu-BDC MOFs. Using Williamson-Hall plots, density dislocation (δ) and strain (ε) induced in MOFs due to crystal imperfection and distortion were computed and their values were in the range of 0.204 cm^2, 0.230 cm^2, and 0.111 cm^2,0.0924 cm^2 for Cu-BDC MOFs and 2-MBIA-Cu-BDC MOFs respectively [9].

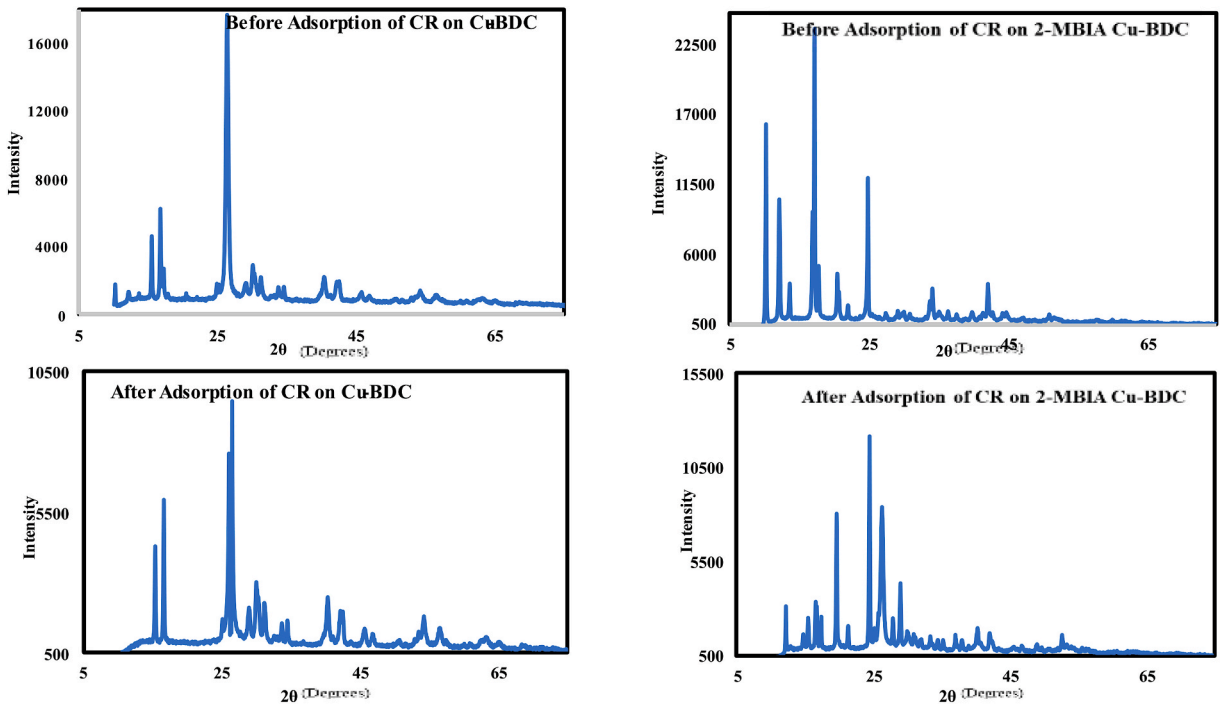

Fig. 1. *p*-XRD spectrum of Cu-BDC MOFs and 2-MBIA-Cu-BDC MOFs before and after adsorption of CR.

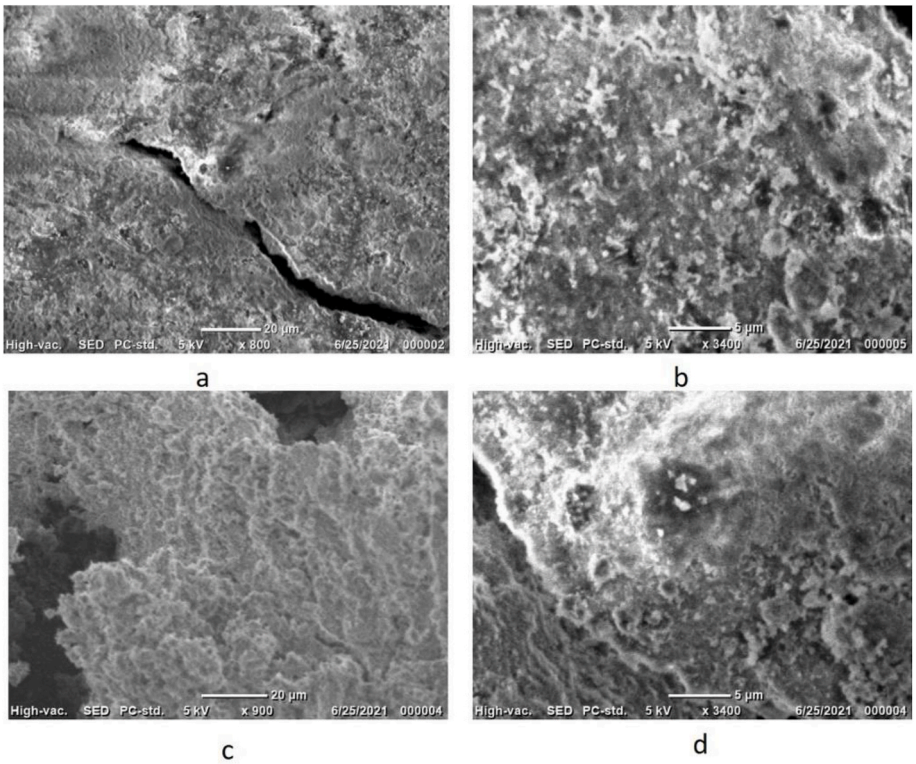

Fig. 2. SEM images of (a) Cu-BDC MOFs (20 µm) (b) Cu-BDC MOFs (5 µm) (c) 2-MBIA-Cu-BDC MOFs (20 µm) (d) 2-MBIA-Cu-BDC MOFs (5 µm).

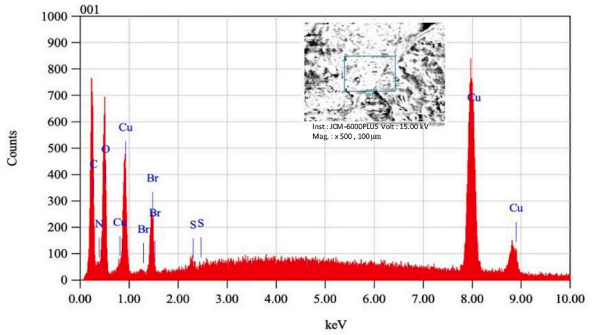

Fig. 3. FE-SEM EDAX spectrum of 2-MBIA-Cu-BDC MOFs (100 µm, Mag: 500).

$$D = \frac{k\lambda}{\beta\,(Cos\,\theta)} \quad (5)$$

where D is the average crystalline size, K is the dimensionless shape factor (0.9), λ wavelength of X-ray, β is the line broadening at FWHM, θ is angle of diffraction.

3.2. FSEM-EDAX

SEM (scanning electron microscope) and EDAX studies were carried out to explore the morphology and elemental composition of newly synthesized 2-MBIA-Cu-BDC MOFs which are shown in Figs. 2 and 3 [27]. It was evident from Fig. 2, that the presence of small crystallites on the surface with pores is due to a specific pattern of assembled organic linkers and metal compounds, therefore, can act as a good adsorbent. Cu-BDC MOFs appeared with fewer particles as shown in Fig. 2 (a and b). However, the current synthesized 2-MBIA-Cu-BDC MOFs nano-size MOFs have exhibited irregular shape morphology with a particle size of 410 nm as shown in Fig. 2 (c and d). It is observed that the addition of 2-MBIA in the organic linker improves the crystalline nature of Cu-BDC MOFs. Besides,

Table 1
Comparison of morphology of MOFs.

Organic Linker	Metal ion	Synthesis method	Reaction Time (hour)	Modified MOF	Morphology	Crystallite size (nm)	Ref
H_2BDC	Cu	Solvothermal	24	Cu-MOF	Cubic	300–500	[1]
Mn-UiO-66@GO-NH2	Mn, Zr	Solvothermal	22	UiO-66	Irregular octahedral	–	[16]
Cd (5-aip) (bpy) Cd (5-hip) (bpy)	Cd	Solvothermal	48	–	Orthorhombic crystal	–	[19]
NH_2IsoBDCH_2,N,N′ (naphthalene −1,5-diyl)di iso nicotinamide,	Co	Solvothermal	72	TMU-69	Nanoplates	100–1600	[24]
NH_2IsoBDCH_2,N,N'-(naphthalene −1,5-diyl) di iso nicotinamide,	Co	Sonication	15	TMU-69	Bulk crystals	100–1300	[24]
NH_2-BDC	Al, Zn, Z r	Solvothermal	20	MIL-101-NH2	Spindle	100–1000	[26]
NH_2-BDC, PVP	Cu	Solvothermal	08	Cu-MOFs	Spherical	236.79	[18]
2-amino-terephthalic acid	Fe	Solvothermal	20	Fe-MIL 88NH_2	Spindle	irregular size	[27]
H_2BDC	Fe	Solvothermal	20	MIL-101	Spindle	100–1000	[28]
BDC	Sn	Hydrothermal	24	Sn-BDC	Rhomboidal	–	[29]
BDC	Cu	Solvothermal	20	Cu-BDC	Non uniform particles	70	present study
2-MBIA, BDC	Cu	Solvothermal	20	2-MBIA-Cu-BDC	Non uniform particles	65.9	Present study

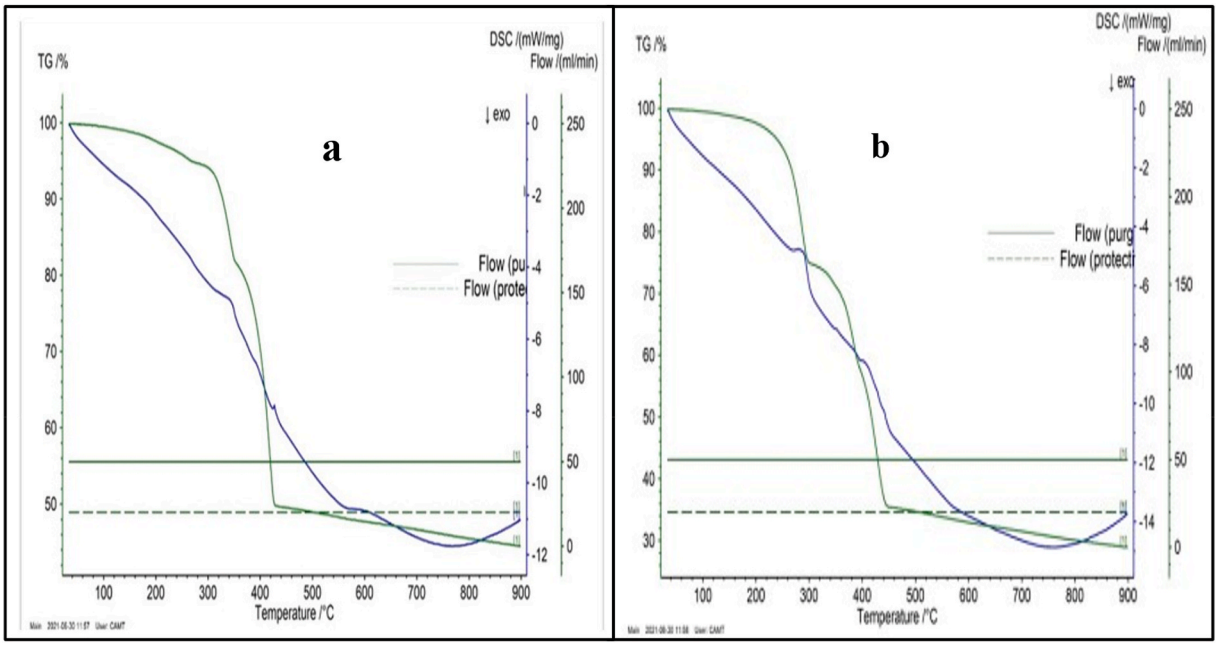

Fig. 4. Thermal gravimetric analysis of (a) Cu-BDC MOFs (b) 2-MBIA-Cu-BDC MOFs.

Table 2
Decomposition products of TGA.

Temperature (°C)	Weight loss percentage			Decomposed products
	Calculated (%)	Experimental (%)	Error (%)	
250–300	19.1	18	1.0	CO_2
300–420	33.9	34	0.1	C_6H_6, C
180–300	22.7	22	0.7	CS_2, H_2O
300–420	43.9	44	0.1	H_2O, CO_2, C_6H_6, NO_2

additive 2-MBIA to the MOFs reduces pore densities on MOFs surface, hence, adsorption efficiency may be decreased. On the other hand, certain reagents and temperatures played a significant role in tuning the morphology of the different metal-organic frameworks and was compared and presented in Table 1. The presence of elements in the organic linker and metal compound of the novel MOFs was evidenced in the FSEM-EDAX as shown in Fig. 3.

3.3. Thermogravimetric studies

Fig. 4 explains the thermal stability and decomposition of Cu-BDC MOFs and 2-MBIA-Cu-BDC MOFs in presence of the N_2 atmosphere in the range of 25–900 °C, with a heating rate of 10 °C/min. The decomposition of Cu-BDC MOFs in Fig. 4(a) has shown CO_2 loss in the range of temperature 200–300 °C and C_6H_6 around 300–420 °C left behind CuO and carbon. From Fig. 4(b), the decomposition firstly starts from 240 to 300 °C with a weight loss of 18% in 2-MBIA-Cu-BDC MOFs which may be attributed to the removal of CS_2, H_2O, molecules, and a further 40% weight loss from 300 to 450 °C indicates the second stage of decomposition with the release of decomposition products like H_2O, NO_2, CO_2, C_6H_6 from the organic linkers BDC and 2-MBIA, left behind CuBr with black char of carbon (Table 2). Thus, the Cu-BDC MOFs thermal stability increases from 180 to 240 °C with the addition of 2-MBIA during the synthesis of 2-MBIA-Cu-BDC MOFs. The chemical decomposition reactions are given below [34,51].

Chemical decomposed reactions' equations.

a) Decomposition reactions of Cu-BDC MOFs

$$[Cu–C_8H_6O_4] \rightarrow CO_2 + [Cu–C_7H_6O_2] \quad \text{i}$$

$$[Cu–C_7H_6O_2] \rightarrow C_6H_6 + + CuO + C \quad \text{ii}$$

b) Decomposition reactions of 2-MBIA-Cu-BDC MOFs

$$[Cu–C_{18}H_{10}NS_2O_6\ Br] \rightarrow CS_2 + H_2O + [\ Cu–C_{17}H_8O_5NBr] \quad \text{iii}$$

$$[Cu–C_{17}H_{10}\ O_5\ Br] \rightarrow H_2O + NO_2 + CO_2 + C_6H_6 + 10C + CuBr \quad \text{iv}$$

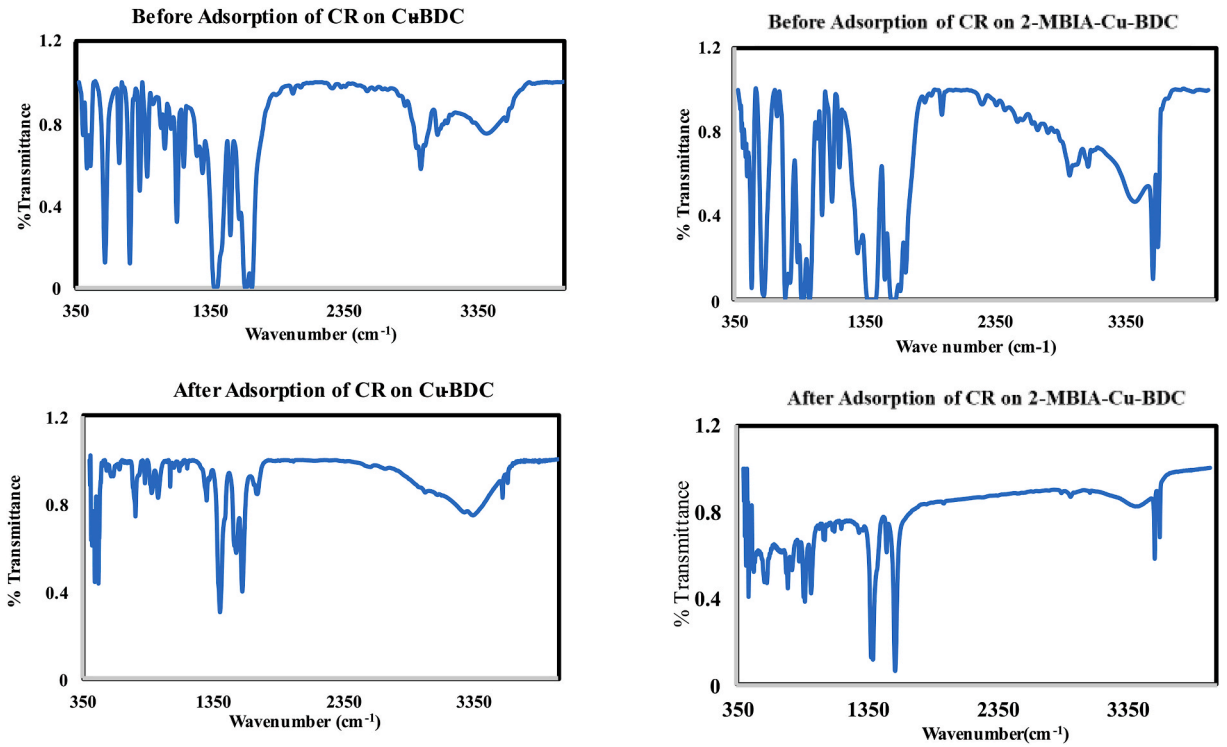

Fig. 5. FTIR spectrum of Cu-BDC MOFs and 2-MBIA-Cu-BDC MOFs before and after adsorption of CR.

3.4. FTIR studies

Fig. 5 explains the functional group, stretching, and bending vibrations of MOFs. The strong vibrational peak at 1511.33 cm^{-1} and 1575.32 cm^{-1} were assigned to symmetric and asymmetric stretching vibrations of –COOH. Peak, 1631.25 cm^{-1} related to –C═O of 2-MBIA and 2931.70 cm^{-1} of –O═C–H, confirm the carboxylic group of 2-MBIA in the novel MOFs synthesized. The peaks at 1623 cm^{-1}, 765 cm^{-1}, 820 cm^{-1} and 589 cm^{-1} declare were attributed to –C═C- aromatic molecules in MOFs [29–33]. The asymmetrical stretching of the –OH group was at 3041 cm^{-1} and peaks at 402 cm^{-1}, 435 cm^{-1}, and 570 cm^{-1} are relevant CuO and Cu–Br bonds. The peak at 2926 cm^{-1} was assigned for aliphatic (C–H) asymmetric stretching vibrations of DMF [35]. There is a slight shift in the peak, observed due to the additive linker 2-MBIA. The peaks at 3600 cm^{-1} were related to (C═N) and the other extra peaks at 1500, 835, and 480 were assigned to δ *N*–H, δ (C═S), and ν (Ni–S) vibrations of 2-MBIA in the novel MOFs, before adsorption of CR.

3.5. pH effect on point of zero charges (PZC) of adsorbent

Surface charge on the adsorbent is the factor that plays a role in adsorption. By determining an effective parameter known as pH_{pzc}, the surface charge of the adsorbent 2-MBIA-Cu-BDC MOFs was investigated using a series of 0.01 N NaCl solutions with 2–3 mg of MOFs, in the range of pH 2-10 adjusted by adding 0.01 N HCl and 0.01 N NaOH. The final pH of all these solutions was measured after attaining the equilibrium for 24 h, as displayed in Fig. 6. The pH_{pzc} 2-MBIA-Cu-BDC MOFs was at a pH of 5 [26].

3.6. Adsorption studies

Dye adsorption on MOFs from the wastewater generally occurs through the dispersion of the dye molecules in the framework resulting in high adsorption capacity and fast kinetics when there was appropriate interaction with the host backbone, also π-π interactions between dye molecules and empty orbitals of the metal ion in MOFs. The optimization of adsorption studies was carried out as below [22,30,46].

3.6.1. Influence of pH on the adsorption

The influence of pH on the adsorption efficiency was investigated in the range of pH 2.0 to 12.0 and is presented in Fig. 7. CR was an anionic dye but has shown negligible adsorption on the surface of both MOFs below the pH of 2. The adsorption of CR increased with an increase in the pH up to 8 for Cu-BDC MOFs, as shown in Fig. 7(a). In contrast, CR adsorption was approximately 46% on 2-MBIA-Cu-BDC MOFs from the pH of 4–8, shown in Fig. 7(b) [36]. Therefore, the pH of 4 was fixed for 2-MBIA-Cu-BDC MOFs and the pH of 8 for Cu-BDC MOFs to measure the adsorption of CR on both MOFs and their adsorption capacity.

3.6.2. Effect of adsorbent dosage

For adsorbent dosage range 5–50 mg, batch experiments were conducted for 100 mL of 50 ppm CR at pH of 4 solutions for 2-MBIA-Cu-BDC MOFs, and pH of 8 solutions for Cu-BDC MOFs and were stirred for 60 min. The sample was collected and centrifuged at 5000 rpm for 15 min and absorbance was measured at 490.4 nm (λ_{max}). The dye percentage adsorbed onto both MOFs surfaces at intervals of time was computed using equation (6) [7,26,36].

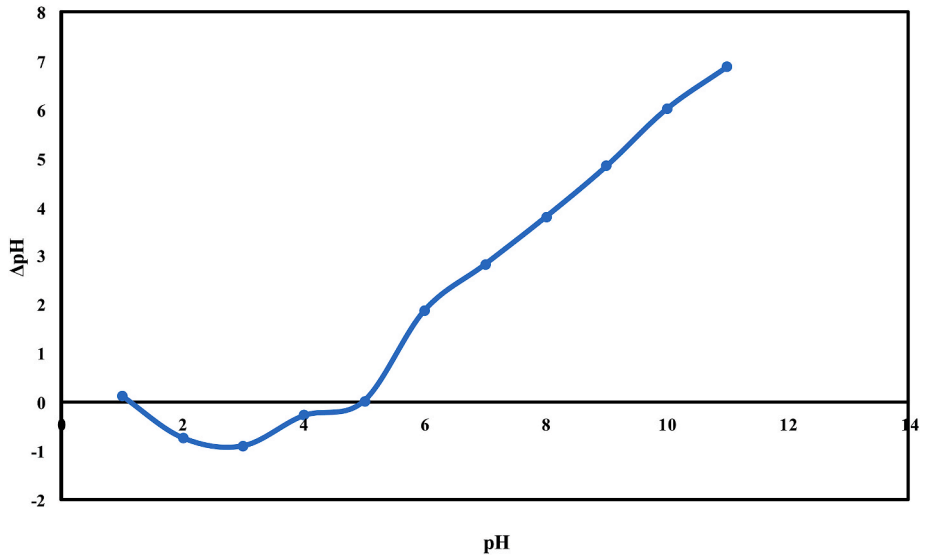

Fig. 6. Effect of pH on PZC of 2-MBIA-Cu-BDC MOFs.

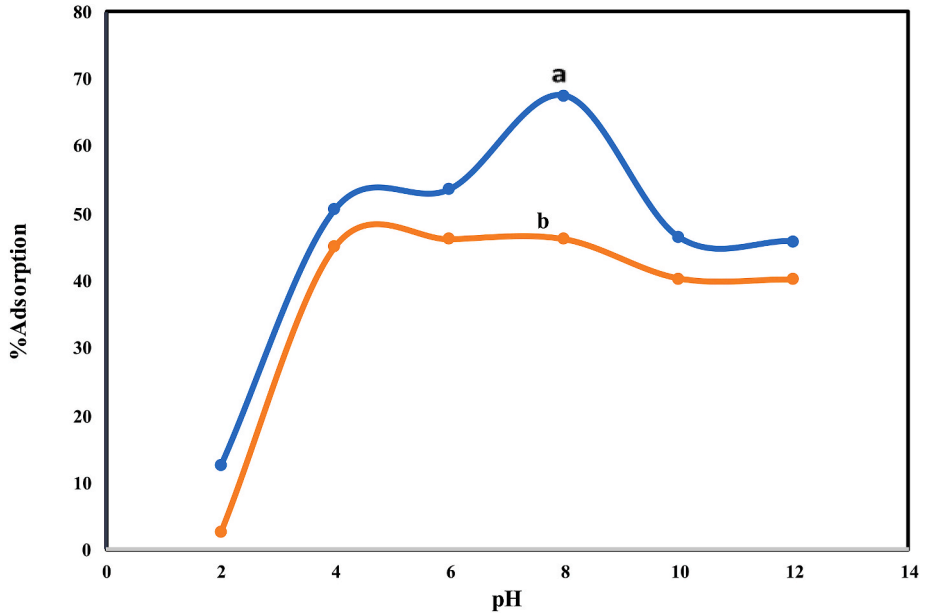

Fig. 7. Effect of pH on adsorption efficiency (a) Cu-BDC MOFs (b) 2-MBIA-Cu-BDC MOFs.

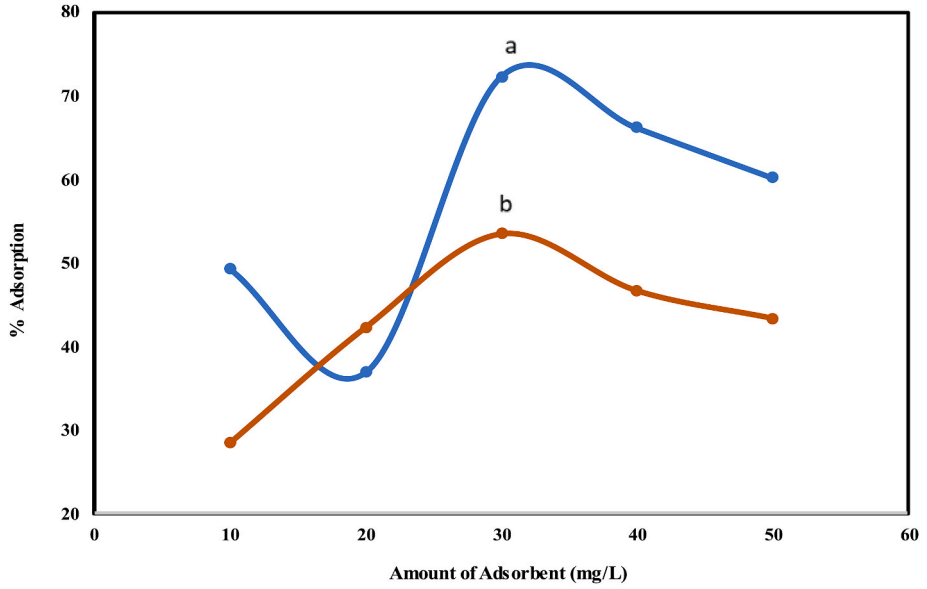

Fig. 8. Effect of adsorbent dosage on a percentage of CR adsorption (a) Cu-BDC MOFs (b)2-MBIA-Cu-BDC MOFs.

$$\%\text{Adsorption} = \frac{(C_0 - C_t)}{C_0} \times 100 \quad (6)$$

where C_0 (mg/L) & C_t (mg/L) are the initial dye concentration and the dye concentration at any time, t respectively. By considering the dye amount before and after the adsorption process, the initial volume, V(L) of CR and mass, m (g) of the adsorbent, the adsorbed amount of dye at equilibrium for the unit mass of adsorbent, q_e (mg/g) was calculated using the following equation (7) [26,36].

$$q_e = \frac{C_0 - C_e}{m} \times V \quad (7)$$

The percentage of dye adsorbed with respect to adsorbent dosage is shown in Fig. 8. It is observed that the percentage of adsorption increases initially with an increase in the adsorbent dosage up to 30 mg caused by increasing the number of active sites and a drastic

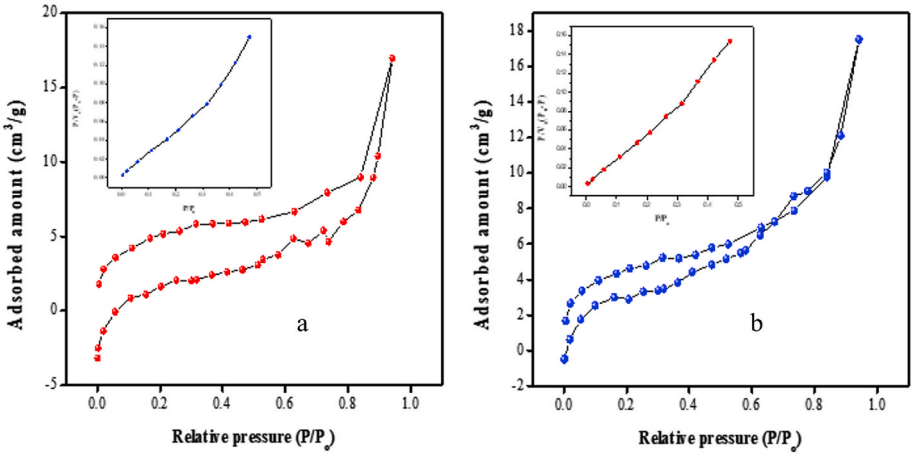

Fig. 9. BET Nitrogen adsorption isotherm. (Inset: BET surface area plot) (a) Cu-BDC MOFs (b) 2-MBIA-Cu-BDC MOFs.

decrease of absorbance for further loading of the adsorbent is due to agglomeration of MOFs particles which in turn decreases active sites and surface area [34–36]. The addition of 2-MBIA to the Cu-BDC MOFs structure reduces surface area, hence, decreasing the adsorption percentage, as evidenced by BET studies.

3.6.3. BET studies

Geometric features of an absorbent were analyzed by measuring BET on the surface area which suggests the availability of a greater number of vacancies that assists in the absorptive removal of toxic pollutants like dyes, metal ions, etc for purification of polluted water. BET surface area of 2-MBIA-Cu-BDC MOFs was found to be 17.02 $m^2\ g^{-1}$ and that of Cu-BDC MOFs was 17.953 $m^2\ g^{-1}$. Its mean pore diameter was 8.48 nm and 5.84 nm, 0.361 $cm^3\ g^{-1}$ and 0.0271 $cm^3\ g^{-1}$ being the total pore volume. Fig. 9 depicts N_2 adsorption/desorption isotherms and also pore size on the surface of both MOFs and falls under type-1 isotherm according to IUPAC classification with mesoporous nature of the surface. 2-Mercaptobenimidazole analogue of Cu-benzene dicarboxylic acid MOFs shown a slight decrease in surface area and can still accommodate the high amount of active material.

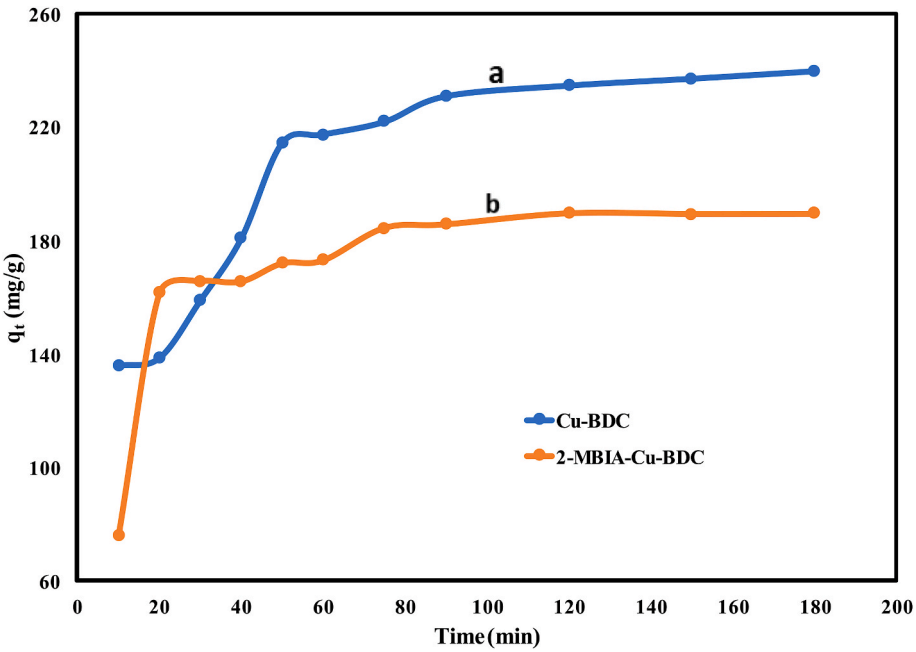

Fig. 10. Adsorption capacity of MOFs with time (a) Cu-BDC MOFs (b) 2-MBIA-Cu-BDC MOFs.

Table 3
Description of non-linear kinetic models.

Kinetic Models	Non-linear Equations
Pseudo First Order Kinetics (PFO)	$qt = qe(1 - (exp - k_1 t)$
Pseudo Second Order Kinetics (PSO)	$qt = \frac{qK_2 t}{1 + q_e k_2 t}$
Elovich Model	$q_t = \frac{1}{\beta} ln(1 + \alpha\beta t)$

Where qe (mg/g) is adsorption capacity at equilibrium; qt (mg/g), adsorption capacity or concentration of solute in a solid phase at time t (min); K_1 (min^{-1}), pseudo-first-order rate constant; K_2 (g/mg min), pseudo-second-order rate constant.

3.7. Adsorption kinetics

Adsorption kinetic studies were carried out using an optimum concentration of 100 ppm dye, 30 mg of sorbent, pH (4) solution for 2-MBIA-Cu-BDC MOFs, and pH (8) for Cu-BDC MOFs. A Sampling of the solution was done in the designed time intervals of 0–150 min. The amount of dye adsorbed for time (q_t) was calculated by using equation (8) [7,26,36].

$$q_t = \frac{C_0 - C_t}{m} \times V \quad (8)$$

Where C_0 and C_t are the concentration of CR at t = 0 and at any time t respectively. It was clear from Fig. 10 that the adsorption rate was quite rapid in the first 20 min for 2-MBIA-Cu-BDC MOFs and 50 min for Cu-BDC MOFs. Further, the adsorption process attains saturation with time in both samples (Fig. 10). This clearly indicates that the adsorption of Congo red dye has taken place on both MOFs. Different kinetic models like PFO, PSO, Elovich, and intraparticle diffusion was used to explore the mechanism of adsorption and their equations were shown in Table .3. It has been observed that CR dye adsorption on Cu-BDC MOFs was 240 mg/g and 189 mg/g on 2-MBIA-Cu-BDC MOFs at 150 min [26,28]. The decline of CR adsorption on 2-MBIA-Cu-BDC MOFs was noticed due to reduction of the surface area results in reducing the availability of the active sites; also, an increase in the pore diameter leads to leaching out of CR dye from the adsorbent when equilibrium was reached. The kinetic and statistical parameters are summarized in Table 5.

3.7.1. Intraparticle diffusion model

Weber–Morris's diffusion model suggests that the linearity of the plot q_t vs $t^{1/2}$ passing through origin implies the sorption mechanism solely governed through intraparticle diffusion which is the rate-limiting step. equation (9) used is given below [26,47].

$$q_t = k_d t^{1/2} + C \quad (9)$$

The intra-particle diffusion (IPD) constant (K_d) and constant (C) was evaluated from the slope and intercept. In Fig. 11. the graph of IPD reveals that the adsorption of CR on MOFs is not only a surface phenomenon from the linear part of the graph; also, a slow diffusion through the inner pores of the adsorbent was evidenced by the flat portion of the graph. However, the larger C value implies greater surface adsorption (Table 4). The intercept, not pass-through origin refers to the degree of boundary layer control over the adsorption of CR and accounted for the different rates of mass transfer that took place at the initial and final stages in the adsorption mechanism. Therefore, it was concluded that IPD may not only be a rate-limiting step but there may be also many mechanisms that work in the sorption process of CR on both MOFs [1,26,28,42,49].

The kinetic and statistical parameters in Table 5, demonstrate the best fit model is PFO since the value of q_e obtained is found to be closer to the experimental value and ARE, RSS, and chi-squares are lower than PSO and Elovich models in the case of 2-MBIA-Cu-BDC MOFs. [28,50]. In contrast, CR adsorption on Cu-BDC MOFs follows Elovich and PFO models by considering the statistical and kinetic parameters and R^2. In a comparison of CR adsorption on both MOFs, it is illustrated that the addition of 2-MBIA in MOF synthesis has reduced the adsorption capacity of Cu-BDC MOFs due to increased pore size and diminish surface volume which were evidenced in BET analysis. The plot of non-linear kinetic models for CR adsorption on MOFs is shown in Fig. 12.

3.8. Adsorption isotherms

For adsorption batch tests, the optimum dose of both MOFs (30 mg) in various concentrations (20–100 ppm) of the dye solution at pH of 4 for 2-MBIA-Cu-BDC MOFs and pH of 8 for Cu-BDC MOFs were maintained and stirred well for 60 min. The absorbance of the centrifuged solution was determined. Langmuir, Freundlich, Temkin, and Sips, Redlich -Peterson non-linear form of isotherms were examined using sorption data to find the effect of 2-MBIA addition on the adsorption of CR on Cu-BDC MOFs under equilibrium conditions at a constant temperature [23,29,33–46]. The non-linear equations used to analyze the adsorption isotherms are placed in Table 6 and its relevant graphs were shown in Fig. 13.

Where q_m (mg/g) is saturated monolayer adsorption capacity, K_L (L/mg) is Langmuir constant, K_F((mg/g) $(L/mg)^{1/n}$) is Freundlich constant, 1/n is Freundlich intensity parameter, q_S (mg/g) is specific adsorption capacity at saturation, K_S (L/mg) is Sips equilibrium constant, n_S is a dimensionless index of heterogeneity, it describes heterogeneity when n_s value lie in between 0 and 1, if $n_s = 1$, the Sips equation reduces to Langmuir equation and implies homogenous adsorption process, K_{RP} (L/g), and α (L/mg) is Redlich-Peterson

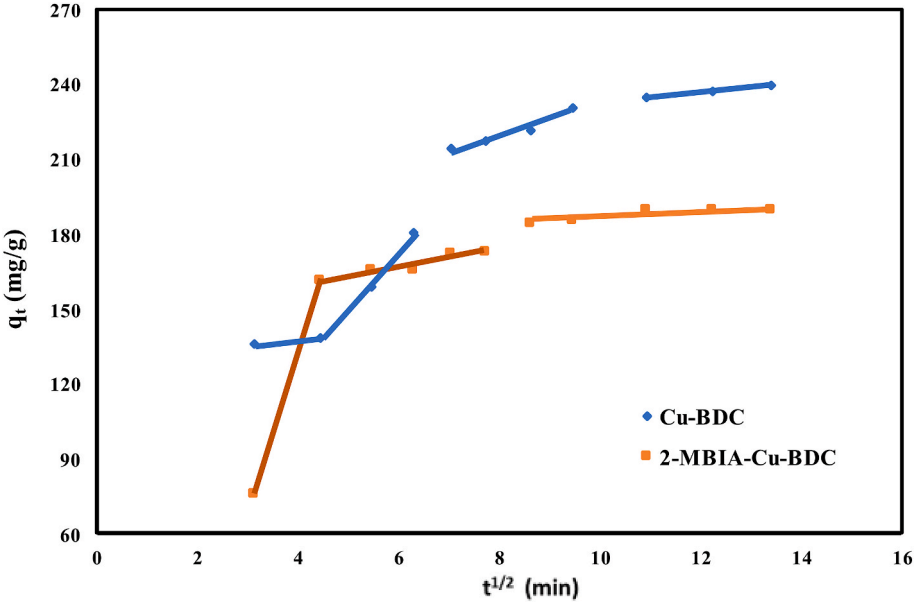

Fig. 11. Plot of Web-Morris Intraparticle diffusion model of CR adsorption on both MOFs.

Table 4
Web Morris Intraparticle Diffusion model parameters.

MOFs	K_d (mg g^{-1} min^{-1})	C mg/g	R^2
Cu-BDC MOFs	23.11	110.087	0.9547
2-MBIA-Cu-BDC MOFs	20.57	98.34	0.9470

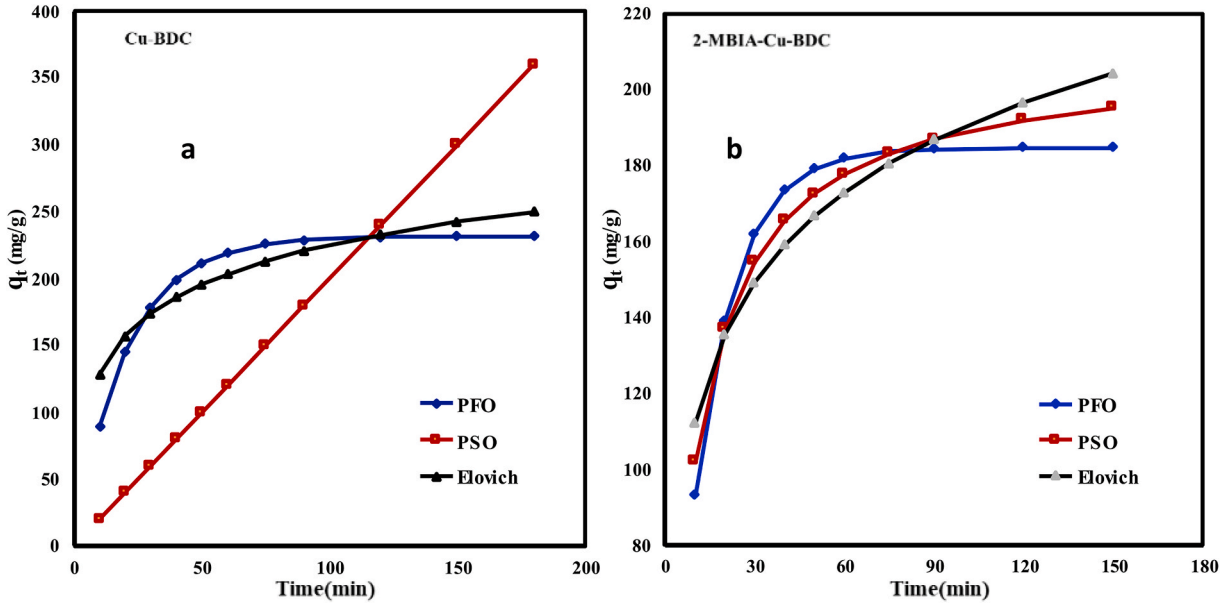

Fig. 12. Plot of Nonlinear kinetic models for CR adsorption on (a) Cu -BDC MOFs (b) 2-MBIA- Cu-MOFs.

isotherm constants, β is an exponent which ranges between 1 and 0. K_T Temkin adsorption constant (L/mg), R (J/mol K) universal constant, T (°C) adsorption temperature, $B_T = \frac{RT}{b}$ is a factor related to heat of adsorption (J/mol). Another feature of the Langmuir isothermal model is separation factor R_L which is dimensionless, as shown below equation (10) [24,26,36,48,49].

Table 5
Kinetic and statistical parameters for adsorption of CR on MOFs.

Kinetic models	Cu-BDC MOFs						2-MBIA-Cu-BDC MOFs					
	Kinetic parameters		Statistical parameters				Kinetic parameters		Statistical parameters			
PFO	**K_1**	**qe**	R^2	RSS	ARE	χ^2 (Chi)	**K_1**	**qe**	R^2	RSS	ARE	χ^2 (Chi)
	0.0490	231.6	0.999	3018.9	0.078	0.015	0.0699	184.7	0.9999	1051.5	0.004	7.6×10^{-5}
PSO	**K_2**	**qe**					**K_2**	**qe**				
	4.3×10^{-5}	214.5	0.9117	91811.6	2.31	17.31	4.6×10^{-4}	208.7	0.9999	1468.8	0.018	6.7×10^{-3}
Elovich	**α**	**β**					**α**	**β**				
	81.25	0.023	0.9999	1539.36	0.029	0.02	85.99	0.029	0.9999	2636.2	0.017	0.048

Table 6
Description of non-linear adsorption isotherm models.

Adsorption isotherm Models	Non-linear Equations
Langmuir	$q_e = \frac{q_{m\ K_L C_e}}{(1 + K_L C_e)}$
Freundlich	$q_e = K_F C_e^{1/n}$
Sips	$q_e = \frac{q_s K_S C_e^{n_s}}{1 + K_S C_e^{n_s}}$
Redlich-Peterson	$q_e = \frac{K_{RP} C_e}{1 + \alpha C_e^{\beta}}$
Temkin	$q_e = \frac{RT}{b} ln(K_T C_e)$

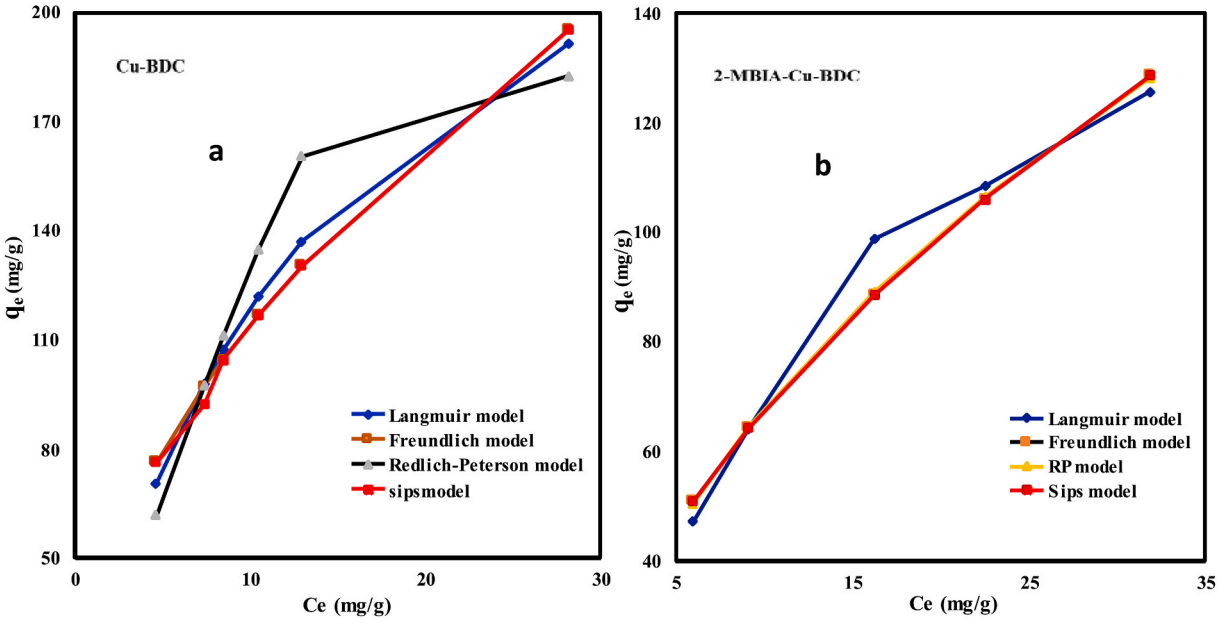

Fig. 13. Plot of non-linear adsorption isotherm models (a) Cu-BDC MOFs (b) 2-MBIA-Cu-BDC MOFs.

$$R_L = \frac{1}{1 + K_L C_0} \quad (10)$$

R_L value implies propitious circumstances to confirm Langmuir adsorption model when unfavourable $R_L > 1$, linear if $R_L = 1$, favourable if $0 < R_L < 1$ and irreversible if $R_L = 0$. C_0 (mg/L) was the initial adsorbate concentration. The R_L of MOFs was given in Table 4 that deduces a favourable adsorption of CR on MOFs. The statistical parameters given in Table .7 suggests that adsorption of CR follows Freundlich and Sips isotherms which are evidenced by high R^2, lower RSS and chi-square values and including n_s, Sips parameter value 0.554 for 2-MBIA-Cu-BDC MOFs. The lower RSS value discloses that the adsorption of CR on Cu-BDC MOFs follows Redlich-Peterson isotherm [45,50]. Finally, we conclude that the best fit isotherm model for 2-MBIA-Cu-BDC MOFs was Freundlich and Sips. The B_T value of Temkin parameter was 82.07 and 45.92 J/mol for 2-MBIA-Cu-BDC MOFs and Cu-BDC MOFs respectively accounts for the adsorption of CR is an exothermic on MOFs. The adsorption capacity of the various adsorbents was shown in Table 8.

Table 7
Isotherm parameters for the adsorption of CR by MOFs.

Isotherm	Cu-BDC MOFs							2-MBIA-Cu-BDC MOFs						
	Model parameters			Statistical parameters				Model parameters			Statistical parameters			
Langmuir	$\mathbf{K_L}$	$\mathbf{R_L}$	$\mathbf{q_L}$	R^2	RSS	ARE	χ^2 (Chi)	$\mathbf{K_L}$	$\mathbf{R_L}$	$\mathbf{q_L}$	R^2	RSS	ARE	χ^2 (Chi)
	0.0693	289.8	0.128	0.9990	4928.8	0.49	0.0418	0.0499	0.193	204.74	0.9994	116.2	0.38	7.0×10^{-5}
Freundlich	$\mathbf{K_F}$	**1/n**	**n**					$\mathbf{K_F}$	**1/n**	**n**				
	34.27	1.919	0.521	0.9998	6410.5	0.21	0.013	18.86	0.554	1.805	1.000	81.50	2.3×10^{-3}	1.2×10^{-5}
Redlich-Peterson	$\mathbf{K_{RP}}$	**β**	**α**					$\mathbf{K_{RP}}$	**β**	**α**				
	12.83	2.1×10^{-9}	6.01	0.9964	1956.38	0.634	0.115	41.94	0.52	1.582	0.9999	82.17	4×10^{-4}	3.9×10^{-6}
Sips	$\mathbf{K_s}$	$\mathbf{n_s}$	$\mathbf{q_s}$					$\mathbf{K_s}$	$\mathbf{n_s}$	$\mathbf{q_s}$				
	0.392	86.33	0.521	0.9998	6410.51	0.21	0.0128	0.277	0.554	66.92	1.000	81.50	4.6×10^{-4}	1.14×10^{-8}
Temkin	$\mathbf{K_T}$	$\mathbf{B_T}$	**b**					$\mathbf{K_T}$	$\mathbf{B_T}$	**b**				
	0.418	30.19	82.07	1.0000	4230.68	2.5×10^{-4}	7.6×10^{-10}	0.465	45.92	53.95	1.0000	150.218	6.38×10^{-5}	8.9×10^{-10}

Table 8
Comparison of adsorption capacity of several materials.

Name of MOFs (Adsorbent)	Dosage of Adsorbent (mg/g)	Adsorption Capacity (mg/g)	Time (min)	Reference number
Co-MOF	30	1760.00	30	[20]
MOF-5/Cu	10	357.42	20	[25]
Fe-MIL-88NH2	15	87.20	60	[27]
Ni–Zn MOF	20	460.90	300	[29]
Co/Fe-BDC	1000	1935.68	100	[30]
Sn(II)-BDC	1000	95.20	250	[35]
Ni/Co-LDH	10	909.20	720	[36]
NH2-MIL 88 (b@CA	20	289.16	480	[37]
NH2-MIL-101@CA	20	228.58	480	[37]
CRGlu–Cu^{2+} MOFs	20	77.60	50	[38]
MIL-101(Cr)	10	1335.04	400	[39]
Sn(II)-BDC MOFs	30	95.20	200	[40]
$[Ni_2F_2(4,4'bipy)_2(H_2O)_2]$ $(VO_3)_2{\cdot}8H_2O$	10	242.10	30	[45]
Cu-BDC	30	243.00	150	Present study
2-MBIA-Cu-BDC	30	189.00	90	Present study

4. Conclusion

A novel metal-organic framework 2-MBIA-Cu-BDC MOFs was synthesized by the solvothermal method and compared the efficiency with regular Cu-BDC MOFs. The addition of 2-Mercaptobenimidazole analogue (2-MBIA) to Cu-BDC MOFs, reduced adsorption capacity due to decreasing surface area and an increase the pore size leads to leaching out dye molecules from the novel MOFs at equilibrium. However, there were no such significant changes in the morphology of the novel MOFs due to the addition of 2-MBIA but the crystallinity of the novel MOFs was found to be improved. Detailed adsorption kinetic studies revealed that the adsorption of Congo red dye on 2-MBIA-Cu-BDC MOFs followed Pseudo first order kinetics and IPD model. The intercept of IPD has described some degree of boundary layer control on adsorption which might be imputed to different mass transfer rate at the initial and final stages of adsorption. The statistical and isotherm parameters have inferred that the adsorption of CR on both MOFs Freundlich and Sips models for 2-MBIA-Cu-BDC MOFs and Redlich-Peterson model for Cu-BDC MOFs. Temkin's isothermal model disclosed that the adsorption process was of an exothermic nature.

Author contribution statement

Malathi Challa: Conceived and designed the experiments; Performed the experiments; Analyzed and interpreted the data; Wrote the paper.

Sampath Chinnam: Analyzed and interpreted the data; Wrote the paper.

Ambika Madalakote Rajanna: Contributed reagents, materials, analysis tools or data.

Basappa C Yallur C Yallur, Apurva Nandagudi, Vinayak Adimule: Contributed reagents, materials, analysis tools or data.

Funding statement

This research did not receive any specific grant from funding agencies in the public, commercial, or not-for-profit sectors.

Data availability statement

No data was used for the research described in the article.

Declaration of interest's statement

There is no conflict of interest declared by authors.

Appendix A. Supplementary data

Supplementary data related to this article can be found at https://doi.org/10.1016/j.heliyon.2023.e13223.

References

[1] R.S. Salama, S.A. El-Hakam, S.E. Samra, S.M. El-Dafrawy, A.I. Ahmed, Modification of the acidic and textural properties of ZSM-5 zeolite by using double mineralizers in synthesis and its catalytic performance in the conversion of methanol to propene, Int. J. Mod. Chem. 10 (2018) 195–207.

[2] Y. Mao, et al., A_2-Fold interpenetrated nitrogen-rich metal-organic framework for rapid and selective adsorption of Congo red, Inorg. Chem. 59 (2020) 8213–8219.
[3] Xuelian Li, et al., Highly efficient biodecolorization/degradation of Congo red and alizarin yellow R by chloroperoxidase from *Caldariomyces fumago*: catalytic mechanism and degradation pathway, I & EC Research 52 (2013) 13572–13579.
[4] S. Chatterjee, S. Dey, M. Sarma, P. Chaudhuri, S. Das, Biodegradation of Congo red by manglicolous filamentous fungus Aspergillus flavus JKSC-7 isolated from Indian sundabaran mangrove ecosystem, Appl. Biochem. Microbiol. 56 (2020) 708–717, https://doi.org/10.1134/S0003683820060046.
[5] V. Russo, et al., Applications of metal-organic frameworks in wastewater treatment: a review on adsorption and photodegradation, Front. Chem. Eng. 2 (2020), 581487.
[6] S.H. Mosavi, R. Zare-Dorabei, M. Bereyhi, Rapid and effective ultrasonic-assisted adsorptive removal of Congo red onto MOF-5 modified by $CuCl_2$ in ambient conditions: adsorption isotherms and kinetics studies, ChemistrySelect 6 (2021) 4432–4439.
[7] F.M. Valadi, A. Ekramipooya, M.R. Gholami, Selective separation of Congo Red from a mixture of anionic and cationic dyes using magnetic-MOF: experimental and DFT study, J. Mol. Liq. 318 (2020), 114051.
[8] K. Iqbal, A. Iqbal, A.M. Kirillov, W. Liu, Y. Tang, Hybrid metal-OrganicFramework/inorganic nanocatalyst toward highly efficient discoloration of organic dyes in aqueous medium, Inorg. Chem. 57 (2018) 13270–13278.
[9] R. Azhdari, S.M. Mousavi, S.A. Hashemi, S. Bahrani, S. Ramakrishna, Decorated graphene with aluminum fumarate metal organic framework as a superior non-toxic agent for efficient removal of Congo Red dye from wastewater, J. Environ. Chem. Eng. 7 (2019), 103437.
[10] S. Tian, S. Xu, J. Liu, C. He, Y. Xiong, P. Feng, Highly efficient removal of both cationic and anionic dyes from wastewater with a water-stable and eco-friendly Fe-MOF *via* host-guest encapsulation, J. Clean. Prod. 239 (2019), 117767.
[11] J. Panda, et al., Adsorptive behavior of zeolitic imidazolate framework-8 towards anionic dye in aqueous media: combined experimental and molecular docking study, J. Mol. Liq. 278 (2019) 536–545.
[12] O. Akeremale, Metal-organic frameworks (MOFs) as adsorbents for purification of dye-contaminated wastewater: a review, J. Chem. Rev. 4 (2022) 1–14.
[13] M. Beydaghdari, F.H. Saboor, A. Babapoor, V.V. Karve, M. Asgari, Recent advances in MOF-based adsorbents for dye removal from the aquatic environment, Energies 15 (2022) 2023.
[14] A.S. Eltaweil, H.M. Elshishini, F.Z.F. Ghatass, G.M. Elsubruiti, Ultra-high adsorption capacity and selective removal of Congo red over aminated graphene oxide modified Mn-doped UiO-66 MOF, Powder Technol. 379 (2020) 407–416.
[15] S. Ghosh, A. Sarkar, S. Chatterjee, H.P. Nayek, Elucidation of selective adsorption study of Congo red using new Cadmium(II) metal-organic frameworks: adsorption kinetics, isotherm and thermodynamics, J. Solid State Chem. 296 (2021), 121929.
[16] M. Hasanzadeh, A. Simchi, H.S. Far, Kinetics and adsorptive study of organic dye removal using water-stable nanoscale metal organic frameworks, Mater. Chem. Phys. 233 (2019) 267–275.
[17] R.J. Kuppler, et al., Potential applications of metal-organic frameworks, Coord. Chem. Rev. 253 (2009) 3042–3066.
[18] A. Ayati, M.N. Shahrak, B. Tanhaei, M. Sillanpaa, Emerging adsorptive removal of azo dye by metal–organic frameworks, Chemosphere 160 (2016) 30–44.
[19] Y. Cui, et al., Metal–organic frameworks as platforms for functional materials, Acc. Chem. Res. 49 (2016) 483–493.
[20] C. Chen, et al., Adsorption behaviors of organic micropollutants on zirconium metal–organic framework UiO-66: analysis of surface interactions, ACS Appl. Mater. Interfaces 9 (2017) 41043–41054.
[21] M.J. Katz, et al., A facile synthesis of UiO-66, UiO-67 and their derivatives, Chem. Commun. 49 (2013) 9449–9451.
[22] F. Ming, et al., Copper-based metal–organic framework nanoparticles for sensitive fluorescence detection of ferric ions, Anal. Methods 11 (2019) 4382–4389.
[23] F. Zarekarizi, A. Morsali, Ultrasonic-assisted synthesis of nano-sized metal-organic framework; a simple method to explore selective and fast Congo Red adsorption Ultrason, Sonochem 69 (2020), 105246.
[24] N. Ayawei, A.N. Ebelegi, D. Wankasi, Modelling and interpretation of adsorption isotherms, J. Chem. (2017), 3039817.
[25] J. Hu, W. Dai, X. Yan, Comparison study on the adsorption performance of methylene blue and Congo red on Cu-BTC, Desalination Water Treat. 57 (2016) 4081–4089.
[26] T. P Krishna Murthy, R. Hari Krishna, M. N Chandraprabha, G. Divyashri, Crasto Vanessa, S.V. Dhanyatha, S. Megha, Swarnima Patil, Glycerol mediated solution combustion synthesis of nano magnesia and its application in the adsorptive removal of anionic dyes, Nano Express 1 (2020), 030018.
[27] J. Yang, et al., Review—temperature dependence of luminescence intensity and decay time in Mn^{4+}-activated oxide phosphors, ECS J. Solid State Sci. Technol. 11 (2022), 056003.
[28] Qiuping Fu, et al., Highly effective and fast removal of Congo red from wastewater with metal-organic framework Fe-MIL-88NH2, J. Solid State Chem. 294 (2020), 121836.
[29] N. Bakhtiari, S. Azizian, Adsorption of copper ion from aqueous solution by nanoporous MOF-5: a kinetic and equilibrium study, J. Mol. Liq. 206 (2015) 114–118.
[30] Jianchuan He, Yao Zhang, Xiaodan Zhang, Yuming Huang, Highly efficient Fenton and enzyme-mimetic activities of NH_2-MIL-88B(Fe) metal organic framework for methylene blue degradation, Sci. Rep. 8 (2018) 1–8.
[31] Z.U. Zango, et al., Response surface methodology optimization and kinetics study for anthracene adsorption onto MIL-88(Fe) and NH_2-MIL-88(Fe) metal-organic frameworks, IOP Conf. Ser. Mater. Sci. Eng. 1092 (2021), 012035.
[32] P. Yadav, A. Yadav, P.K. Labhasetwar, Sustainable adsorptive removal of antibiotics from aqueous streams using Fe_3O_4-functionalized MIL101(Fe) chitosan composite beads, Environ. Sci. Pollut. Res. 29 (2022) 37204–37217.
[33] A. Ghosh, G. Das, Green synthesis of Sn(II)-BDC MOF: preferential and efficient adsorption of anionic dyes, Microporous Mesoporous Mater. 297 (2020), 110039.
[34] Yi Liu, et al., Fabrication of CoFe-MOF materials by different methods and adsorption properties for Congo red, J. Mol. Liq. 360 (2022), 119405.
[35] T.L. Tan, H. Nakajima, S.A. Rashid, Adsorptive, Kinetics and regeneration studies of fluoride removal from water using zirconium-based metal organic frameworks, RSC Adv. 10 (2020) 18740–18752.
[36] M. Gouamid, M.R. Ouahrani, M.B. Bensaci, Adsorption Equilibrium, kinetics and thermodynamics of methylene blue from aqueous solutions using Date Palm Leaves, Energy Proc. 36 (2013) 898–907.
[37] F.M. Valadi, A. Ekramipooya, M.R. Gholami, Selective separation of Congo Red from a mixture of anionic and cationicdyes using magnetic-MOF: experimental and DFT study, J. Mol. Liq. 318 (2020), 114051.
[38] Shi-Wen Lva, et al., A novel and universal metal-organic frameworks sensing platform for selective detection and efficient removal of heavy metal ions, Chem. Eng. J. 375 (2019), 122111.
[39] A. Ghosh, G. Das, Facile synthesis of Sn(II)-MOF using waste PET bottles as an organic precursor and its derivative SnO2 NPs: role of surface charge reversal in adsorption of toxic ions, J. Environ. Chem. Eng. 9 (2021), 105288.
[40] H. Hu, J. Liu, Z. Xu, L. Zhang, B. Cheng, W. Ho, Hierarchical porous Ni/Co-LDH hollow dodecahedron with excellent adsorption property for Congo red and Cr (VI) ions, Appl. Surf. Sci. 478 (2019) 981–990.
[41] C. Huang, B. Cai, L. Zhang, C. Zhang, H. Pan, Preparation of iron-based metal-organic framework @ cellulose aerogel by in situ growth method and its application to dye adsorption, J. Solid State Chem. 297 (2021), 122030.
[42] F. Pu, X. Liu, B. Xu, J. Ren, X. Qu, Miniaturization of metal–biomolecule frame works based on stereo selective self-assembly and potential application in water treatment and as antibacterial agents, Chem. Eur J. 18 (2012) 4322–4328.
[43] T. Shen, J. Luo, S. Zhang, X. Luo, Hierarchically mesostructured MIL-101 metal–organic frameworks with different mineralizing agents for adsorptive removal of methylorange and methylene blue from aqueous solution, J. Environ. Chem. Eng. 3 (2015) 1372–1383.
[44] M. Yang, Q. Bai, Q, Flower-like hierarchical Ni-Zn MOF microspheres: efficient adsorbents for dye removal, Colloids Surf., A 582 (2019), 123795.
[45] J. Zolgharnein, S.D. Farahani, M. Bagtash, S. Amani, Application of a new metal-organic framework of $[Ni_2(F)2\ (4,4'\text{-bipy})2\ (H_2O)_2]\ (VO_3)_2.\ 8H_2O$ as an efficient adsorbent for removal of Congo red dye using experimental design optimization, Environ. Res. 182 (2020), 109054.

[46] B.H. Hameed, D.K. Mahmoud, A.L. Ahmad, Equilibrium modeling and kinetic studies on the adsorption of basicdye by a low-cost adsorbent: coconut (Cocos nucifera) bunch waste, J. Hazard Mater. 158 (2008) 65–72.
[47] R. Farouq, N.S. Yousef, Equilibrium and kinetics studies of adsorption of copper (II) ions on natural biosorbent, Int. J. of Chem. Eng. and Appl. 6 (2015) 319–324.
[48] T. Madrakian, A. Afkhami, M. Ahmadi, Adsorption and kinetic studies of seven different organic dyes onto magnetite nanoparticles loaded tea waste and removal of them from wastewater samples, Spectrochim. Acta, Part A. 99 (2012) 102–109. M.
[49] T.P. Krishna Murthy, B.S. Gowrishankar, R. Hari Krishna, M.N. Chandraprabha, R. Sreenivasa Rao, Influence of fuel nature on dye adsorption efficiency of solution combustion derived zinc oxide nanoparticles: a comparative study, Mater. Res. Express 6 (2019), 055512.
[50] Lakshmi Narayani, et al., Mechanism of high temperature induced phase transformation and magnetic properties of Mn_3O_4 crystallites, J. Magn. Magn Mater. 476 (2019) 268–273.
[51] H.H. Willard, L.L. Merritt Jr., J.A. Dean, F.A. Settle Jr., Instrumental Methods of Analysis, first ed., Wadsworth Publishing Company, USA, 1986.